

Connectivity and Dynamics of Neuronal Networks as Defined by the Shape of Individual Neurons

Sebastian Ahnert

*Theory of Condensed Matter, Cavendish Laboratory,
University of Cambridge, JJ Thomson Avenue, Cambridge CB3 0HE, UK*

Luciano da Fontoura Costa*

*Instituto de Física de São Carlos,
Universidade de São Paulo,
Av. Trabalhador São Carlense 400,
Caixa Postal 369, CEP 13560-970,
São Carlos, São Paulo, Brazil*

(Dated: 7 September 2007)

Neuronal networks constitute a special class of dynamical systems, as they are formed by individual geometrical components, namely the neurons. In the existing literature, relatively little attention has been given to the influence of neuron shape on the overall connectivity and dynamics of the emerging networks. The current work addresses this issue by considering simplified neuronal shapes consisting of circular regions (soma/axons) with spokes (dendrites). Networks are grown by placing these patterns randomly in the 2D plane and establishing connections whenever a piece of dendrite falls inside an axon. Several topological and dynamical properties of the resulting graph are measured, including the degree distribution, clustering coefficients, symmetry of connections, size of the largest connected component, as well as three hierarchical measurements of the local topology. By varying the number of processes of the individual basic patterns, we can quantify relationships between the individual neuronal shape and the topological and dynamical features of the networks. Integrate-and-fire dynamics on these networks is also investigated with respect to transient activation from a source node, indicating that long-range connections play an important role in the propagation of avalanches.

‘Nothing in excess.’ (Delphic proverb)

I. INTRODUCTION

Many discrete systems in nature can be modeled in terms of networks which explains the remarkable development of the field of complex networks research over the last decade (e.g. [1, 2, 3, 4, 5]). Because such systems involve a large number of elements exchanging mass, energy or information, their representation as a graph or network is intrinsic. A wide range of complex systems, from the Internet to protein-protein interaction, has been successfully mapped and studied in terms of complex networks (e.g. [6]). The connectivity of a network also influences the properties of dynamical processes which may take place on it. This relationship between topology and dynamics is of particular interest in many networks [7] including neuronal ones.

Despite the many applications of complex networks research, little attention has been given to systems in which the overall connectivity is affected (or even defined) by the geometrical features of the individual constituent elements. Indeed, the majority of works addressing structure and dynamics in complex networks tends

to equate the structure with the topology of the networks, without regarding the geometry of the involved components. While it is true that many networks do not have a geometrical basis — such as author collaboration and disease transmission networks, as well as the Internet — some important complex systems are formed by elements with a well-defined geometry which influences or even defines the emerging connectivity and dynamics. Such *morphological networks* include protein-protein interaction as well as the biological neuronal networks in the central nervous systems (CNS) of animals, which are called *morphological neuronal networks*. In such networks which are the result of spatial interactions between geometrical constituent elements, the information about the geometry of the original elements may not be available to the researcher. This is often the case in protein-protein interaction and neuronal networks, where only the connectivity between the nodes is provided.

A particularly important example of morphological networks are neuronal systems, which can be represented as directed networks with each neuron being a node and each synapse a directed edge. The resulting connectivity and dynamics are closely related to the geometry of the involved neurons. Indeed, a large number of morphological neuronal types (e.g. [8]) have been identified in the CNS of vertebrates as well as more primitive animals (e.g. insects). Morphological neuronal types range from cells as simple as the bipolar neurons of the retina to the intricate Purkinje neurons of the cerebellum. Because the

*Electronic address: luciano@if.sc.usp.br

neuronal shapes are highly variable, no consensus exists on how they should be categorized.

The contribution of the individual morphology of neurons to the overall network connectivity mostly occurs in two ways: (a) the biochemical differentiation of neuronal types constrains the respective geometries and connections (e.g. a Purkinje cell will never exhibit radial organization); and (b) the growth of each dendrite or axon takes into account influences from the surrounding environment, such as electric fields and gradients of concentration of molecules. Therefore, the shape of a neuron in the CNS is a consequence of both *nature* (i.e. the biochemical content associated to cell differentiation) and *nurture* (i.e. the effects of the surrounding environment). The spatial distribution of the bodies of the neurons (called somata or perykaria) also plays an important role in defining the overall connectivity. It is important to bear in mind that neuronal systems are highly plastic, undergoing structural and dynamical changes during their whole lifetime. Therefore, it is particularly important to consider the interrelationship between neuronal structure and dynamics in growing networks.

Here we provide the first systematic investigation on the relationship between the geometry and dynamics of growing morphological networks. Because of the stochastic nature of biological neuronal networks, it becomes essential to consider a large number of realizations in order to obtain meaningful measurements of topology and dynamics. Therefore, we keep the total number of involved parameters as small as possible, focussing on those which are clearly related to neuronal shape and connectivity. First, we restrict our investigation to 2D neurons and neuronal networks. Such a simplification is justified by the fact that several real neurons such as retinal ganglion cells, Purkinje and even the basal dendritic structure of the ubiquitous pyramidal cells are mainly planar. Next, we adopt prototypical radial neurons involving a central region (axon) from which a given number of dendrites with the same length (spokes) emerge. This model implies as parameters: the number and length of dendrites, angular distribution of the dendrites, and the radius of the central region. By assuming a fixed dendritic area for all neurons, the length of the dendrites can be related to their number, so that one of these parameters can be omitted.

Once the types of neurons are defined, the networks can be obtained by progressively placing new neuronal cells and establishing connections whenever a part of a dendrite touches an axon. We use a uniform random distribution of the position of the cells. Before being added to the network, each cell is rotated by a uniformly random angle. Therefore, the only additional parameters implied by the network growth are the current number of added cells and the size of the space along which the neurons are distributed.

In order to investigate the relationship between structure and dynamics in these networks, we make a series of different measurements. In order to express the topology

of the networks we determine the degrees of the nodes, their clustering coefficient, Garlaschelli's symmetry index [9], as well as the size of the largest connected component in the network. The dynamics of the respective networks is obtained in terms of integrate and fire dynamics [10, 11]. More specifically, each node is understood as a neuron which integrates the received activation until a threshold is reached, in which case a spike is produced as output. It has been verified [12, 13] that integrate-and-fire complex networks can undergo avalanches of activations when stimulated from individual nodes, with the type of connectivity substantially affecting the dynamics. More specifically, such avalanches have been related to specific concentric organization of the network connectivity [12, 13]. Given the source node i , the nodes which are at topological distance 1 from i are called the first concentric level, the neurons which are at distance 2 constitute the second hierarchical level, and so on. Avalanches are related to the existence of concentric levels with a large number of nodes. More specifically, if a concentric level h contains many nodes while the preceding and subsequent levels are less populated, the firing of neurons in the level h tends to induce overall activation of the neighboring levels, which then propagates through the whole network. In the case of undirected networks it is possible to obtain a simple equivalent model of the original network, formed by a chain of a few equivalent nodes across the hierarchical levels [12, 13]. This model allows predictions of avalanche characteristics, such as the required activation ratios [13], even for symmetrized versions of directed networks. Such an approximation is particularly justified when the original directed network involves a relatively high degree of symmetric connections, as is the case for our morphological networks with large number of spokes n .

Possible interdependencies between the structure and dynamics of the networks are investigated by considering the Pearson correlation of these measurements.

We begin with a brief overview of the basic concepts of complex networks theory and morphological neuronal networks.

II. BASIC CONCEPTS

A. Complex Networks Topology

Directed networks are defined by a set of N nodes and E edges which can be represented by an adjacency matrix A , such that its element $a_{ij} = 1$ indicates the presence of a directed edge from node i to node j , while $a_{ij} = 0$ expresses its absence.

The topological properties of a network can be quantified and characterized in terms of a comprehensive set of measurements [5]. In this work we consider the following features: (i) in- and out-degree; (ii) clustering coefficient; (iii) Garlaschelli's symmetry index; and (iv) size of the largest connected component in the network. More

specifically, we consider the averages and standard deviations of the measurements taken over the whole networks. Each of these measurements, as well as the motivation for their adoption, are described in detail as follows:

Average Node In- and Out-degree: The in- and out-degree of an individual node i corresponds to the number of edges leading to and from that node. These measurements can be obtained directly from the adjacency matrix as:

$$a_i^{in} = \sum_{j=1}^N a_{ji} \quad (1)$$

$$a_i^{out} = \sum_{j=1}^N a_{ij} \quad (2)$$

The average in- and out-degrees, $\langle k_i^{in} \rangle$ and $\langle k_i^{out} \rangle$, taken over the whole network, are identical and provide a quantification of the overall degree of connectivity in the network.

Average Clustering Coefficient: The clustering coefficient of a node i measures how interconnected the neighbors of node i are. It does so by counting the number of connections between neighbors of i and dividing it by the number of possible connections - in other words, by the number of pairs of neighbors. In directed networks this can be written as:

$$c_i = \frac{n}{d_i(d_i - 1)} \quad (3)$$

where $d_i = \sum_j (a_{ij} + a_{ji})$ is the number of neighbors of node i and $n = \sum_{j,k} [1 - (1 - a_{ij})(1 - a_{ji})][1 - (1 - a_{ik})(1 - a_{ki})](a_{jk} + a_{kj})$ is the number of directed edges between those nodes. Note that $0 \leq c_i \leq 1$, with $c_i = 0$ indicating a total lack of interconnectivity between the neighbors and $c_i = 1$, i.e. all neighbors are connected to each other. Another version of the clustering coefficient for directed networks, which takes the variety of directed topological environments into account, has been reported in [14].

Garlaschelli's Symmetry Index: Introduced by Garlaschelli [9], this measurement quantifies the symmetry of connections between pairs of nodes relative to an Erdős-Rényi network of the same size and density. Let E be the total number of directed edges in the network, and E_b be the total number of bidirectional (symmetric) edges, and define the ratios $r = E_b/E$ and $a = E/(N^2 - N)$. The symmetry index is then given by:

$$\rho = \frac{r - a}{1 - a} \quad (4)$$

Size of the Largest Connected Component: At any time during the growth of a network, it is of interest to quantify the overall path connectivity among the existing nodes. This can be done by measuring the size

C of the largest connected component in the network. More specifically, a *connected component* [22] is a subgraph such that each node can be reached from any other node through at least one path.

Because the dynamics of complex neuronal networks is defined by the concentric organization (e.g. [12, 15]) of their topology, we also consider three hierarchical measurements, namely the hierarchical number of nodes, the hierarchical degree and the intra-ring degree. Given an undirected network, the concentric level h of a node i is defined as the set of nodes which are separated from i by a shortest path of length h . The maximum value of h is H . The *hierarchical number of nodes* at level h , with respect to a reference i , is equal to the number of nodes at that level. The *hierarchical degree* of a node i at level h corresponds to the number of edges between the levels h and $h + 1$. The *intra-ring degree* of a node i at level h is the number of edges between nodes of that level.

B. Morphological Networks

Morphological networks are networks formed by a spatial distribution of individual geometrical components [16] with connections between them defined by their overlap. For instance, a biological neuronal network is composed of neurons with a specific geometry given by their dendritic and axonal arborizations. Morphological networks can be classified into subcategories with respect to: (i) the individual shape of the basic elements, (ii) the degree of homogeneity of such elements in the network (e.g. networks containing a single or multiple type of individual shape), and (iii) the way in which these elements are spatially distributed. Each of these cases is discussed below in detail:

Individual Neurons: The individual shape of the network elements can closely mirror real elements (e.g. by using images of neurons) or they can take a more abstract form (e.g. by using some pattern generation method). In the case of neural morphological networks, the shape of the neurons is composed of dendrites and axons. As neuronal connections (i.e. synapses) extend from axon to dendrite, such networks are directed. The shape of the elements can be represented in a discrete form, such as digital images or a continuous form, e.g. by (possibly piecewise) continuous curves. The geometrical properties of the basic elements in the network can be quantified by using a series of measurements such as area, perimeter, fractal dimension, symmetry, etc.

Degree of Homogeneity: Morphological networks may involve single or multiple basic elements, possibly involving geometrical transformations (e.g. rotation or scaling).

Spatial Distribution: Morphological networks are created by distributing the element shapes in space and considering their overlap. Several types of distributions can be considered, e.g. uniformly random or preferential to specific positions (e.g. a normal distribution centered at

a given point).

In order to keep the number of involved parameters and degrees of freedom as small as possible, allowing statistically representative simulations, we choose the following representation of individual neurons: (a) the dendrites are represented by a star of spokes with uniform angle between them; (b) the total length of the dendrites is fixed and therefore independent of the number of spokes; (c) the axon, which corresponds to the soma, is a circle of fixed radius at the center of the star. Identical neurons, rotated randomly, are used to build each network. The neurons are placed sequentially at uniformly random positions within the unit square.

Figure 1 illustrates a simple morphological network obtained for $N = 20$ and $n = 3$. Each neuron corresponds to a circle (the soma and axon) from which $n = 3$ spokes emanate. The neurons, which are placed with varying rotations, are identified by their respective central points. The network obtained is shown in black, superimposed into the original morphological structure. Observe that neuron number 4 remains isolated. All other 19 cells belong the largest strongly connected component.

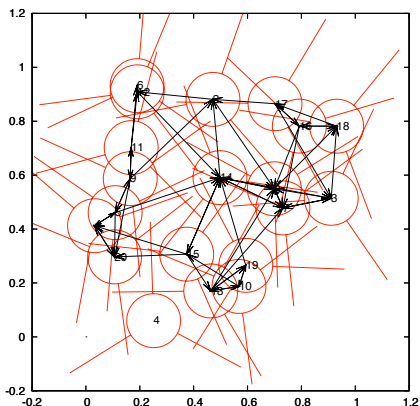


FIG. 1: An example of morphological network obtained by considering $N = 20$ and $n = 3$. A directed connection is established whenever a dendrite crosses the axon of another neuron.

C. Integrate-and-Fire Complex Neuronal Networks

In this work, the dynamics of the morphological networks is simulated by considering the integrate-and-fire neuronal model (e.g. [10]), which incorporates the most important elements characterizing real neuronal networks, namely integration of the activation received by each cell along time, related to the biological phenomenon of *facilitation* [8], and a non-linear transfer function. Figure 2 illustrates the main components of

the integrate-and-fire neuronal cell. The incoming axons are connected to the dendrites of the neuronal cell i , their signals being added by the integrator Σ at each time step and stored in the internal state $S(i)$. In this work we assume equal synaptic weights. Once the value of $S(i)$ reaches a given threshold $T(i)$, the cell produces a spike and its internal state $S(i)$ is cleared. The activation conveyed by the axons is fixed at intensity 1, reflecting the constant amplitude of the action potential characteristic of real neuronal networks.

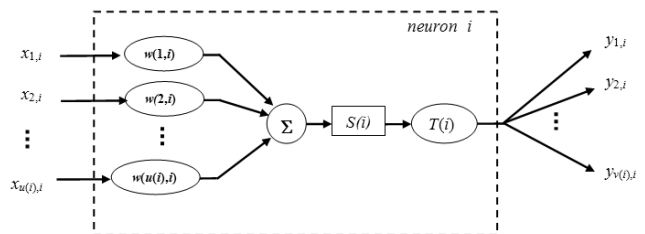


FIG. 2: The integrate-and-fire model of neuronal cell dynamics adopted in this work incorporates $v(i)$ incoming connections with respective weights, $u(i)$ outgoing links, an integrator Σ , the internal memory $S(i)$ storing the time-integrated activation, and the non-linear transfer function (a hard limit is adopted in this work). Every time the internal activation $S(i)$ exceeds the threshold $T(i)$, the neuron fires, generating a spike of fixed intensity 1 and clearing the internal activation.

Though other types of activations can be considered, in the present work we activate the networks through a *source node*. More specifically, one of the network nodes is chosen and injected with constant activation equal to 1. All neurons have the same threshold $T(i) = T$, and all synaptic weights are fixed at 1.

The networks studied here are of sizes $N = 200$ and 400 , with a varying number of dendrites (i.e. spokes). The radius of the soma was 0.0625 and the total length of the dendrites was 0.5. Only the largest connected components are considered for the analysis of the integrate-and-fire dynamics.

The overall integrate-and-fire dynamics unfolding in a network can be characterized in several ways (e.g. [10, 12, 17]). Here, we consider the internal activation and spikes produced by each neuron over time. More specifically, we will focus attention on the transient phenomenon of *avalanches of spikes* (e.g. [12, 17, 18]) which may take place during the initial activation of the network. Because we are considering the largest connected component in each network, the activation arriving at the source eventually reaches all the neurons in the networks. Interestingly, such an activation may progress either gradually or involve an abrupt onset of spikes, i.e. an avalanche. The intensity and sharpness of these avalanches are defined by the concentric properties of the topology of the respective networks [12, 17]. After an avalanche, the to-

tal number of spikes in the network tends to exhibit well-defined oscillations [17].

The type of activation transition can be predicted [19] by considering the three following ratios derived from the hierarchical number of nodes $n_h(i)$, hierarchical degrees $k_h(i)$, and intra-ring degrees $a_h(i)$

$$s1_h(i) = \frac{k_h(i)}{n_{h+1}(i)} \frac{1}{T} \quad (5)$$

$$s2_h(i) = \frac{a_h(i)}{n_h(i)} \frac{1}{T} \quad (6)$$

$$s3_h(i) = \frac{k_h(i-1)}{n_{h-1}(i)} \frac{1}{T} \quad (7)$$

$$(8)$$

The quantity $s1_h(i)$, called *forward activation ratio*, quantifies the intensity of the transfer of activation from the neurons in level h into level $h + 1$ after most of the neurons in level h have fired (because of degree regularity, the nodes within each concentric level tend to fire at similar times). The *reflexive activation ratio* $s2_h(i)$ expresses how much of the activation of the neurons at level h remains at that same level. The transfer of activation from level h to level $h - 1$ is quantified in terms of the *backward activation ratio* $s3_h(i)$. All ratios are normalized with respect to the threshold T of every cell so that ratio values of 1 indicate a full transfer of the received activation.

It is important to note that the propagation of the avalanches is influenced by the finite size and local topology of the networks. Consider a perfectly regular but finite orthogonal lattice. For any given node, the concentric layers of neighbours surrounding it will be characterized by levels with progressively increasing number of nodes, up to a point where this number starts to decline again as a consequence of the finite size of the network. This maximum (see [13] for the complete analytical results), plays an important role in the formation of avalanches. Several other types of complex networks have been shown to undergo avalanches under specific parameter configurations [12, 13]. It is also possible to design networks which will never produce avalanches, e.g. by having more uniform distributions of nodes along the concentric levels. Real-world neuronal systems are often organized into modules with sometimes only a few dozens of neurons, which is in line with the size of networks in our models.

III. CHARACTERIZATION OF THE TOPOLOGY

Figure 3 shows the average out-degree $\langle k_i^{out} \rangle$ (a), the average clustering coefficient $\langle c_i \rangle$ (b), the symmetry coefficient ρ (c) as well as the size of the largest connected component divided by the number of neurons (d) in terms of the time t (which is equal to the number of placed

neurons) for 50 morphological networks with $n = 1$ to 20 spokes (identified by different colors).

It is clear from Figure 3(a) that the average in-degree increases roughly quadratically as additional neurons are incorporated into the network. In addition, the average in-degree also increases with the number of spokes up to $n = 5$, decreasing thereafter. As shown in Figure 3(b), the average clustering coefficient tends to increase linearly with the number of added neurons t . It also increases with the number of spokes n up to $n = 10$, before leveling off at higher values of n . The symmetry index, shown in Figure 3(c), remains nearly constant with t but increases steadily with the number of spokes n . This reflects the fact that for large numbers - and thus a high angular density - of spokes, there is a high probability that if the axon of neuron A is reached by the dendrite of neuron B, the opposite will also be true. The size of the largest connected component C always converges to 1, with faster convergence being observed for larger values of n . Except for $n = 1$, most of the neurons will be part of the largest connected component for $t > 100$.

The concentric organization of the adopted morphological networks ($N = 200$), known to play an important role in the integrate-and-fire dynamics, is illustrated in Figure 4 with respect to the average standard deviation of the hierarchical number of nodes $n_h(i)$, hierarchical degrees $k_h(i)$, and intra-ring degrees $a_h(i)$.

Figure 3 makes it clear that all three measurements behave similarly, exhibiting a peak near the middle concentric level. In addition, larger number of spokes tend to increase the total number H of concentric levels in the networks, which goes from about 6 for $n = 1$ to 13 for $n = 20$. Similar results were obtained for $N = 400$.

Figure 5 shows the mean values of the three considered concentric measurements for $n = 1, 3, 5, 10$ and 20. It is clear from this figure that the increase of the number of spokes implies a larger number of concentric levels as well as smoother distributions of measurements along the h -axis. Furthermore it is evident that the dispersions of each configuration decrease with n . Because the integrate-and-fire dynamics is defined by the concentric organization of the network, the distribution of the configurations shown in Figure 5 implies that the adopted networks are poised to yield distinct types of avalanche dynamics.

In order to obtain additional insights about the latter issue, namely the type of activation transitions during the transient regime, we calculated also the three activation ratios (Eqs. 5– 6) for each of the configurations of morphological networks. Table I shows the mean and standard deviation values of the three activation ratios obtained for the two concentric levels associated to the largest number of original nodes assuming $T = 7$. It should be recalled that these three ratios are defined for undirected networks, so that the morphological structures were symmetrized before the respective calculations. It has been verified that the ratios obtained for the symmetrized versions of a directed network still capture

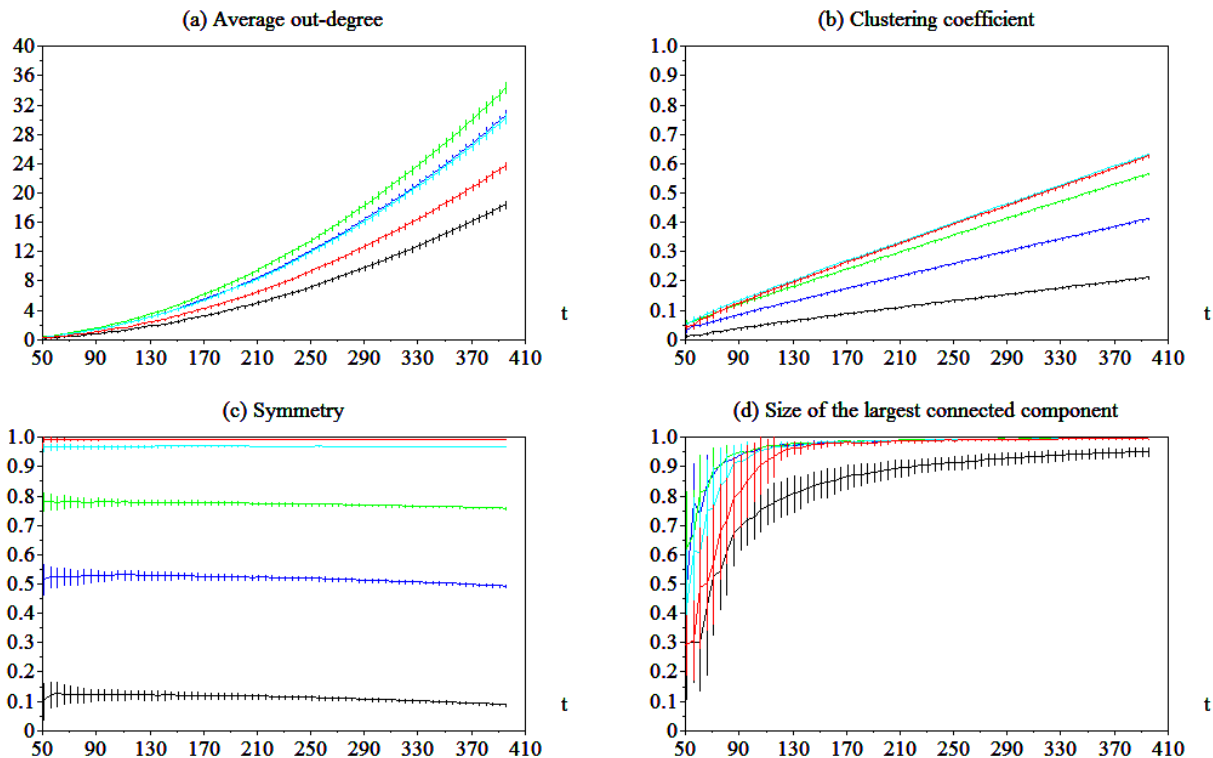


FIG. 3: The average out-degree $\langle ok \rangle$ (a), average clustering coefficient $\langle cc \rangle$ (b), symmetry coefficient ρ (c) as well as the size of the largest connected component divided by the number of neurons (d) in terms of the time obtained along the growth of 50 morphological networks with $n = 1$ to 20 spokes ($n = 1$ in black, $n = 3$ in blue, $n = 5$ in green, $n = 10$ in cyan, $n = 20$ in red).

to a good deal the integrate-and-fire important dynamical features.

Most networks involve at least one ratio with values smaller or near 1, suggesting that the activation in these networks proceed in a relatively gradual manner. Indeed, the activations tend to be more gradual for the configurations with larger number of spokes.

IV. CHARACTERIZATION OF THE DYNAMICS

In this section we investigate the transient activation dynamics of the morphological networks with respect to several configurations. Figure 6 illustrates the spikegram (a) and total number of spikes (b) obtained for a network with $N = 200$, $n = 3$ and $T = 3$.

The spikegram in Figure 6(a) shows the occurrence of a spike (shown in white) over time (vertical axis) for each of the $N = 200$ neurons in the network (horizontal axis). As the network is fed from node 1, a few neurons (the most immediate neighbors of node 1) start sporadic firing, up to nearly $t = 50$, when most of the neurons begin producing spikes, signaling the occurrence of an avalanche. Figure 6(b) shows the total number of spikes along time. In the case of this specific example, this signal involves three preliminary peaks of spiking, followed

by the avalanche. The total number of spikes tends to undergo regular oscillations after the avalanche.

As predicted by the respective three activation ratios calculated for each of the networks configuration (see previous Section), gradual activations and almost complete lack of avalanches were observed for $T = 7$, as illustrated in Figure 7. In other words, the configurations of morphological networks considered in the present work incorporate concentric organizations which imply the transient activation to be distributed in a relatively gradual manner.

So far we have considered identical model neurons with uniformly distributed spokes of equal length. However, real-world biological neuronal systems are characterized by the coexistence of short and long range connections. The latter interconnect diverse cortical modules and regions [8, 20]. In order to investigate the effect of long-range connections in our morphological networks, we added a number of random edges. Figure 4 shows the three main hierarchical measurements obtained for the same network used to produce Figure 6, but with 20% E new randomly chosen directed edges. It is evident from this figure that the incorporation of additional edges completely changes the concentric organization of morphological networks, by reducing the total number of concentric levels H (compare with Fig. 4) as well as implying sharper peaks in the hierarchical number of nodes

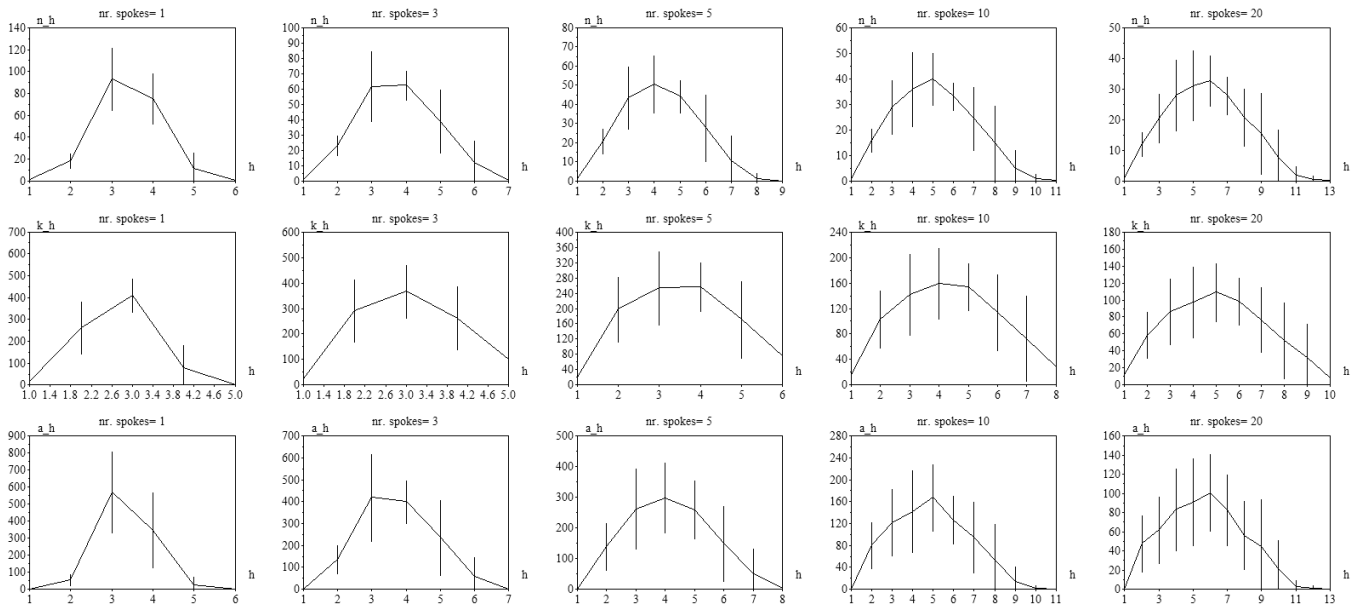


FIG. 4: The hierarchical number of nodes $n_h(i)$, the hierarchical degrees $k_h(i)$ and the intra-ring degrees $a_h(i)$ obtained for the morphological networks with $N = 200$ and $n = 1, 3, 5, 10$ and 20 spokes.

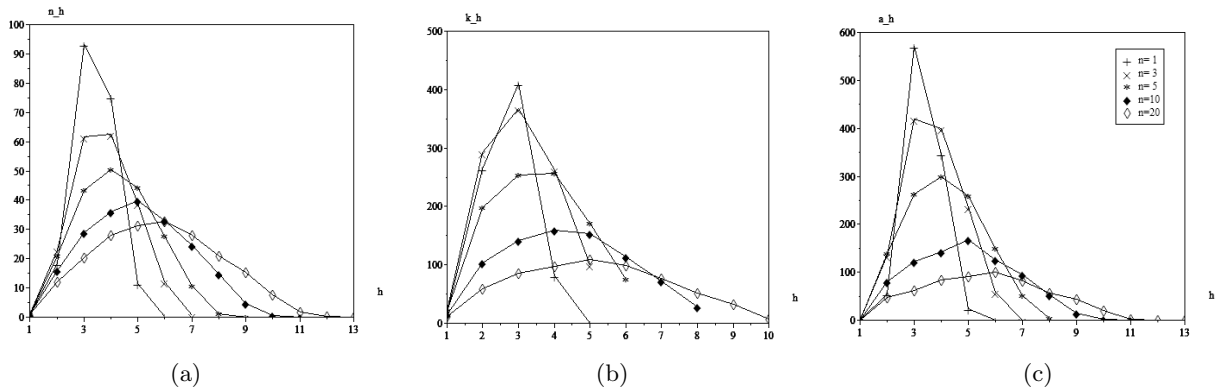


FIG. 5: Superposition of the mean values of the three considered concentric measurements for $n = 1, 3, 5, 10$ and 20 .

and intra-ring degrees signatures.

Table II gives the mean and standard deviation values of the three activation ratios obtained for the 50 morphological networks with 20% E additional edges and $T = 7$ respectively to the two concentric levels containing the largest number of nodes. It should be observed that, as a consequence of the smaller diameter of the networks with 20% E additional edges, the level with the second highest number of nodes contains only a few nodes. Relatively to Table I, we can see that the addition of edges implied in substantially larger values for all the three ratios, predicting sharper and more intense avalanches (confirmed experimentally). Observe that both Tables I and II refer to $T = 7$. Such a major change in the activation ratios is a direct consequence of the drastic influence of the additional edges over the concentric organization of the

respective morphological networks. Even more intense changes have been obtained for larger number of added edges.

The above results imply that morphological networks involving short and long-range connections are substantially more likely to exhibit avalanches of activation than morphological networks involving only short-range connections. Such a finding presents important potential implications for neuroscience, especially because it shows that the activation of morphological networks, including their susceptibility to avalanches, can be controlled by the density of short and long-range links.

n	$s1(first)$	$s1(second)$	$s2(first)$	$s2(second)$	$s3(first)$	$s3(second)$
$n = 1$	2.27 ± 0.43	1.57 ± 0.53	2.01 ± 0.22	1.24 ± 0.41	4.27 ± 1.28	2.08 ± 1.66
$n = 3$	2.46 ± 0.48	2.42 ± 0.66	2.42 ± 0.24	2.04 ± 0.27	3.48 ± 1.32	2.38 ± 0.96
$n = 5$	2.16 ± 0.42	1.96 ± 0.42	2.17 ± 0.28	1.95 ± 0.28	2.63 ± 0.75	2.21 ± 0.82
$n = 10$	1.71 ± 0.36	1.55 ± 0.25	1.52 ± 0.22	1.43 ± 0.20	1.91 ± 0.41	1.81 ± 0.53
$n = 20$	1.30 ± 0.26	1.29 ± 0.30	1.17 ± 0.19	1.05 ± 0.15	1.51 ± 0.31	1.25 ± 0.30

TABLE I: The mean and standard deviations of the activation ratios $s1$, $s2$ and $s3$ considering the concentric levels with the first and second highest number of nodes in the morphological networks with $n = 1, 3, 5, 10$ and 20 . $T = 7$.

n	$s1(first)$	$s1(second)$	$s2(first)$	$s2(second)$	$s3(first)$	$s3(second)$
$n = 1$	3.53 ± 0.73	1.18 ± 0.53	2.54 ± 0.26	1.93 ± 0.32	5.60 ± 0.89	3.50 ± 3.50
$n = 3$	5.45 ± 0.69	1.15 ± 0.21	3.28 ± 0.33	1.61 ± 0.54	5.77 ± 0.73	5.49 ± 4.65
$n = 5$	4.60 ± 0.74	1.07 ± 0.38	2.96 ± 0.35	1.66 ± 0.50	4.85 ± 0.74	2.97 ± 3.07
$n = 10$	2.82 ± 1.07	1.44 ± 0.76	2.06 ± 0.23	1.49 ± 0.28	3.40 ± 0.66	2.26 ± 0.76
$n = 20$	2.55 ± 0.73	1.42 ± 0.64	1.61 ± 0.19	1.17 ± 0.27	2.33 ± 0.49	2.65 ± 0.66

TABLE II: The mean and standard deviations of the activation ratios $s1$, $s2$ and $s3$ considering the concentric levels the first and second highest number of nodes in the morphological networks with 20% E additional edges and $n = 1, 3, 5, 10$ and 20 . $T = 7$.

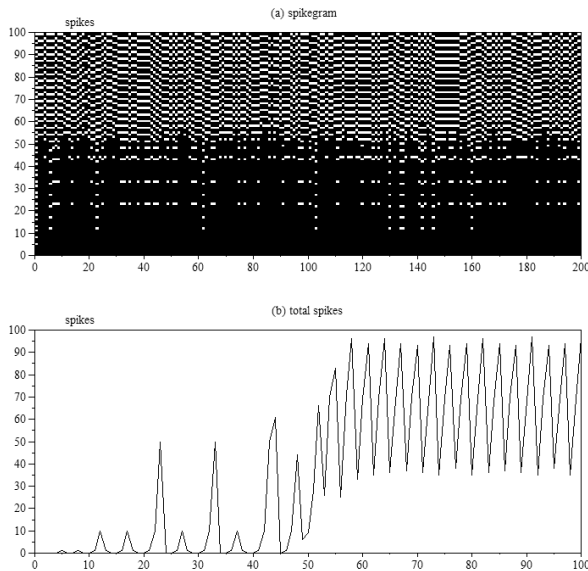


FIG. 6: The spikegram (a) and total number of spikes along time (b) obtained for a morphological network with $N = 200$, $n = 3$ and $T = 3$.

V. RELATING STRUCTURE AND DYNAMICS

Having investigated the integrate-and-fire dynamics for several configurations of morphological networks, our attention is now focused on the particularly relevant issue of relating the structural and dynamical aspects of the considered networks.

Three measurements of each avalanche were extracted automatically: (i) its onset time t_i ; (ii) the mean of the total number of spikes after the avalanche takes place $\langle N_s \rangle$, and (iii) the respective standard deviation σ_{N_s} . The avalanches had to be detected before such measure-

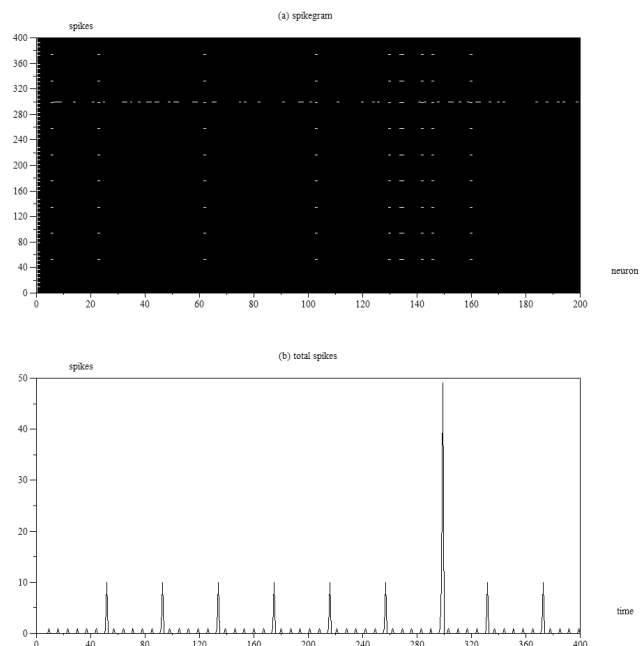


FIG. 7: The spikegram (a) and total number of spikes along time (b) obtained for a morphological network with $N = 200$, $n = 3$ and $T = 7$.

ments could be calculated. This was achieved by thresholding the total number of spikes with signals at one fifth of the maximum height. A total of 500 time steps was considered.

Figure 9 shows the scatterplots of $\langle N_s \rangle$ against $s1$ (a), $s2$ (b), $s3$ (c), as well as the product $(s1)(s2)(s3)$, obtained for $N = 200$, and $T = 3$ for all values of n . This figure shows that the mean intensity of the avalanches tends to increase steeply with the activation ratios and then saturate at a value of about 65. This results shows

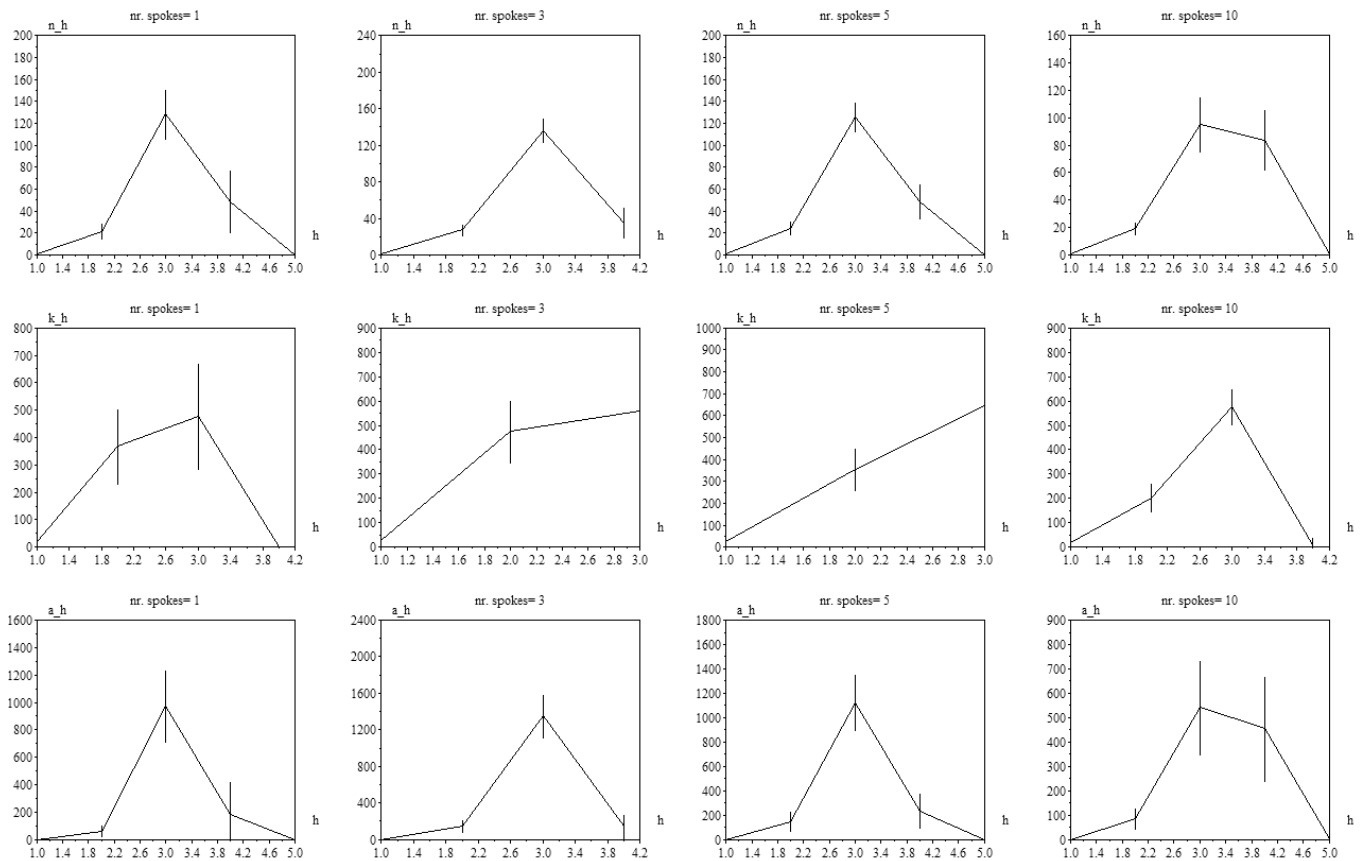


FIG. 8: The hierarchical number of nodes $n_h(i)$, the hierarchical degrees $k_h(i)$ and the intra-ring degrees $a_h(i)$ obtained for the morphological networks with $N = 200$ and $n = 1, 3, 5, 10$ and 20 spokes and 20% additional edges.

that important features of the integrate-and-fire dynamics, such as the average intensity of the avalanches, are intrinsically related to the respective structural properties of the network, here represented by the three activation ratios, which are ultimately derived from the concentric organization. No relationships have been identified between the activation ratios and the other two avalanche measurements.

VI. CONCLUDING REMARKS

The intersection between complex networks and neuronal networks, which has been called *complex neuronal networks*, represents one of the most challenging and promising research areas because it allows neuroscience to be revisited while considering the relationship between structured connectivities such as small-world and scale-free and the respectively obtained dynamics. The current article has addressed this important paradigm with respect to more biologically realistic networks, called *morphological networks*, whose connectivity is defined as a consequence of the shape and distribution of geometrical neuronal cells. By assuming a uniformly random spatial

distribution of geometrically simple neurons consisting of a circular axon and a set of straight dendrites radiating from the soma with uniform angles, it was possible to keep the number of involved parameters as small as possible, allowing the systematic investigation of the effect of the shape of the neurons on the overall topological properties of the resulting networks as well as on the respective integrate-and-fire dynamics. Several interesting results were obtained:

Characterization of the Topology of Morphological Networks in Terms of Traditional Measurements: The topology of the considered morphological networks was characterized in terms of several measurements, including average out-degree, clustering coefficient, symmetry index, and size of the largest connected component. We found that networks obtained by considering neurons with larger number of dendrites tended to exhibit greater symmetry and larger connected components. The average out-degree and clustering coefficient tended to increase with the number of dendrites up to a maximum, decreasing thereafter.

Characterization of the Topology of Morphological Networks in Terms of Hierarchical Measurements: The concentric organization of the morphological networks, as re-

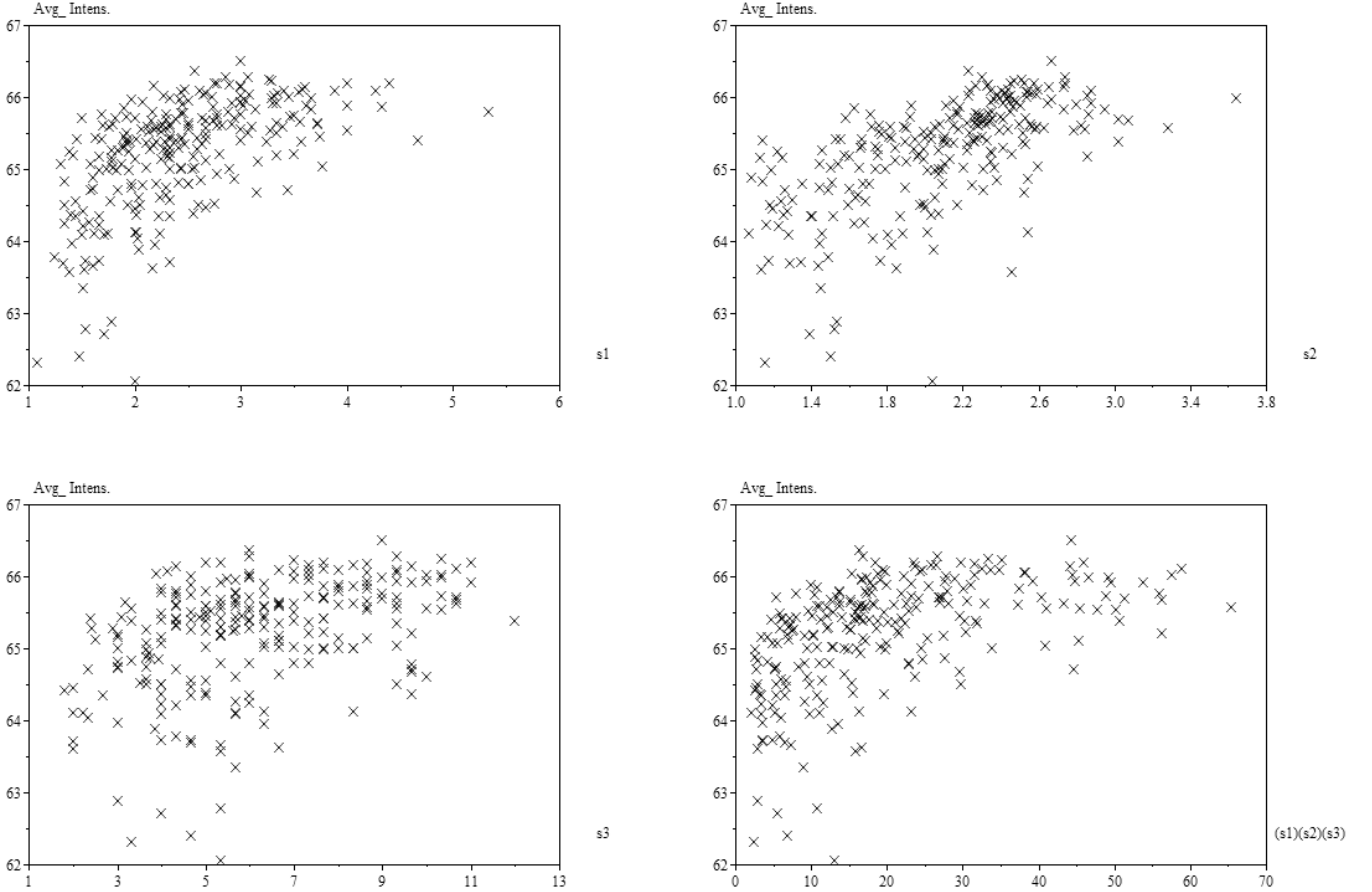


FIG. 9: The scatterplots of the average total number of spikes along time ($N = 200$ and $T = 3$) and respective activation ratios.

vealed by the hierarchical number of nodes, hierarchical degree and intra-ring degree, exhibited several concentric levels, yielding respective signatures characterized by a peak nearly the intermediate level. The gradual distribution of these measurements along the concentric level suggests more gradual activation of the respective networks.

Prediction of the Type of Activation of the Networks: The concentric organization of a network has been found to define important features of the respective integrate-and-fire dynamics [12]. We considered the three activation indices introduced in [19] in order to predict the type of activation of the network. The higher the value of such ratios — which are obtained from the hierarchical number of nodes, hierarchical degree and intra-ring degree, the higher the probability of getting abrupt activation of the network and onset of avalanches. Because the activation ratios for the concentric levels with the largest number of nodes are particularly small, the morphological networks considered in this work are expected to undergo relatively smooth dissemination of the activation received from a source node. Such a type of dynamics was experimentally confirmed.

Investigation of Morphological Networks Involving Short- and Long-Range Connections: Because biological neuronal networks are known to incorporate short- and long-range connections, we repeated our investigations of structure and dynamics considering morphological networks involving also long-range dynamics. It was found that the incorporation of additional connections can change drastically the concentric organization of morphological networks, implying substantial changes also in the respective integrate-and-fire dynamics. In particular, it was found that the addition of 20% random directed edges reduced substantially the number of concentric levels while increasing the activation ratios. The so-obtained morphological networks were found to undergo sharp activation, with onset of avalanches. Such a finding implies that the way in which biological networks are activated can be controlled by the ratio between short- and long-range connections, with morphological networks involving only short-range connections undergoing more gradual activation.

Characterization of the Activation Dynamics in Terms of the Average Intensity of Avalanches and Structure-Dynamics Relationships: A specific methodology was de-

veloped in order to automatically identify the presence of avalanches from the total number of spikes signatures in terms of time. This also allowed the identification of the initiation time and average and standard deviation of the total number of spikes after the occurrence of the avalanches. In order to relate this dynamical behavior to the topology of the networks we investigated possible relationships between the activation ratios (derived from the concentric organization) and initiation time of avalanches, and the average and standard deviation of the total number of spikes after their respective onset. It was verified that the average of the total number of spikes after the avalanches tend to increase steeply with any of the three activation ratios, saturating at a maximum value. No relationships were observed between the ratios and the other two avalanche features.

Possible future directions of research include the consideration of neurons with non-uniformly distributed spokes, neurons with higher branching orders, as well as different types of neurons in the same network and non-uniformly distributed neurons. It would also be interesting to consider integrate-and-fire dynamics with internal activation decay [21].

List of Symbols

Γ = a graph or complex network;
 N = total number of nodes in a network;
 E = total number of edges in a network;
 K = the adjacency matrix of a complex network;
 $k(i)$ = degree of a network node i ;
 $ik(i)$ = in-degree of a network node i ;

$ok(i)$ = out-degree of a network node i ;
 $cc(i)$ = clustering coefficient of a network node i ;
 C = the size of the largest strongly connected component in the network;
 L = the size of the workspace used to build the morphological networks (i.e. $L \times L$);
 $n(i)$ = the number of spokes (dendrites) of a neuron i ;
 $r(i)$ = the radius of the soma (also axon);
 $S(i)$ = the current internal activation of neuron i ;
 $T(i)$ = the threshold of neuron i ;
 $u(i)$ = the number of incoming connections at neuron i ;
 $v(i)$ = the number of outgoing connections of neuron i ;
 H = the total number of concentric levels in a network;
 $n_h(i)$ = the number of hierarchical nodes at level h of neuron i ;
 $k_h(i)$ = the hierarchical degree at level h of neuron i ;
 $a_h(i)$ = the intra-ring degree at level h of neuron i ;
 $s1_h(i)$ = the forward activation ratio at level h of neuron i ;
 $s2_h(i)$ = the reflexive activation ratio at level h of neuron i ;
 $s3_h(i)$ = the backward activation ratio at level h of neuron i .

Acknowledgments

Luciano da F. Costa thanks CNPq (301303/2006-1) and FAPESP (05/00587-5) for sponsorship.

-
- [1] R. Albert and A. L. Barabási, *Rev. Mod. Phys.* **74**, 47 (2002).
[2] S. N. Dorogovtsev and J. F. F. Mendes, *Advs. in Phys.* **51**, 1079 (2002).
[3] M. E. J. Newman, *SIAM Rev.* **45**, 167 (2003).
[4] S. Boccaletti, V. Latora, Y. Moreno, M. Chavez, and D. Hwang, *Phys. Rep.* **424**, 175 (2006).
[5] L. da F. Costa, F. A. Rodrigues, G. Travieso, and P. R. V. Boas, *Advs. in Phys.* **56**, 167 (2007).
[6] L. da F. Costa, O. N. O. Jr., G. Travieso, R. A. Rodrigues, P. R. V. Boas, L. Antiqueira, M. P. Viana, and L. E. C. da Rocha (2008), arXiv:0711.3199.
[7] L. da F. Costa (2005), arXiv:q-bio/0503041.
[8] L. R. Squire, F. E. Bloom, S. K. McConnell, J. L. Roberts, N. S. Spitzer, and M. J. Zigmond, *Fundamental Neuroscience* (Academic Press, 2003).
[9] D. Garlaschelli and M. I. Loffredo, *Phys. Rev. Letts.* **93**, 268701 (2004).
[10] C. Koch, *Biophysics of Computation* (Oxford, 1998).
[11] C. Koch and I. Segev, *Methods of Neuronal Modeling* (The MIT Press, 1998).
[12] L. da F. Costa (2008), arXiv:0802.0421.
[13] L. da F. Costa (2008), <http://hal.archives-ouvertes.fr/hal-00258893/en/>.
[14] G. Fagiolo, *Phys. Rev. E* **76**, 026107 (2007).
[15] L. da F. Costa (2008), arXiv:0802.1272.
[16] L. da F. Costa and T. M. Manoel, *Neuroinformatics* **1**, 65 (2003).
[17] L. da F. Costa (2008), arXiv:0801.3056.
[18] M. Kaiser, M. Goerner, and C. C. Hilgetag, *New J. Phys.* **9**, 110 (2007), arXiv:0802.2508.
[19] L. da F. Costa (2008), hal-00258893, <http://hal.archives-ouvertes.fr/hal-00258893/fr/>.
[20] S. Zeki, *Inner Vision* (Oxford University Press, 1999).
[21] L. da F. Costa (2008), arXiv:0801.4684.
[22] It is important to observe that, in the case of directed graphs, the terminology *strongly connected components* should be preferred.